Available at www.sciencedirect.com

ScienceDirect

journal homepage: www.elsevier.com/locate/ijhydene

Hydrogen generation by hydrolysis of zinc powder aerosol

Hans H. Funke[a,*], *Henry Diaz*[a], *Xinhua Liang*[a], *Casey S. Carney*[a], *Alan W. Weimer*[a], *Peng Li*[b]

[a]*Department of Chemical and Biological Engineering, University of Colorado, ECCH 111, Boulder, CO 80309, USA*
[b]*Department of Earth and Planetary Sciences, University of New Mexico, Albuquerque, NM 87131, USA*

ARTICLE INFO

Article history:
Received 7 February 2007
Received in revised form
15 December 2007
Accepted 24 December 2007
Available online 8 February 2008

Keywords:
Water splitting
Zinc powder
Hydrogen
Aerosol reaction
Thermogravimetric analysis
Hydrolysis

ABSTRACT

The hydrolysis of zinc powder was studied in an aerosol to determine if high conversions are feasible at short residence times and high dispersions. This reaction is the low temperature hydrogen formation step in a two step zinc/zinc oxide based thermo-chemical cycle for water splitting using solar energy. Zinc particles with an average size of 158 nm were reacted with water vapor to form hydrogen and zinc oxide in an aerosol flow tube reactor at ambient pressure (82 kPa) between 653 and 813 K and a water concentration of 3%. The highest conversion observed in the flow system was about 24% at 813 K and a gas residence time of ~0.6 s. Non-isothermal thermogravimetric analysis (TGA) indicated that complete conversion of zinc to zinc oxide could be achieved for longer residence times. An activation energy of 132 ± 27 kJ/mol was calculated from the TGA experiments using a model-free isoconversional method. Standard reaction models did not describe the data so an empirical order of reaction rate law was used instead. Reaction rates in the aerosol flow reactor were higher than those calculated from the TGA measurements, likely due to lower mass and heat transfer resistances in the aerosol.

1. Introduction

Hydrogen can be produced by splitting water using thermo-chemical cycles and solar heat. One promising approach uses a two-step cycle with the Zn/ZnO redox system [1,2]:

$$ZnO \rightarrow Zn + \tfrac{1}{2} O_2$$
(high temperature solar decomposition), (1)

$$Zn + H_2O \rightarrow ZnO + H_2$$
(low temperature water splitting). (2)

The high temperature decomposition of zinc oxide to form zinc metal and oxygen requires a temperature of about 2073 K which is feasible with a solar reactor [3–5]. The zinc formed in situ is initially in the vapor phase and fast quenching of the product stream has been shown to form a fine zinc powder in the nanometer size range [5,6]. Other pathways for the high temperature formation of zinc from zinc oxide include the reaction with methane [6,7] or carbothermal reduction with solid carbon sources [8–10]. Both approaches require lower temperatures than the thermal decomposition of pure zinc oxide but do not provide a closed cycle since an external carbon source is necessary.

The zinc metal powder formed in the high temperature step can then be collected, stored if necessary, and oxidized off-line with water above 663 K to generate hydrogen and zinc oxide. The zinc oxide will be recycled in the high temperature reaction.

The hydrolysis reaction is strongly exothermic (~110 kJ/mol), but the formation of a protective zinc oxide layer prevents rapid conversion in bulk samples. For example, Berman and Epstein reacted molten zinc with steam and

*Corresponding author. Fax: +1 303 492 4341.
E-mail address: funke@colorado.edu (H.H. Funke).
0360-3199/$ - see front matter © 2008 International Association for Hydrogen Energy. Published by Elsevier Ltd. All rights reserved.
doi:10.1016/j.ijhydene.2007.12.061

found that zinc oxide crusts formed that slowed further reaction of the zinc [11]. A more fundamental approach was used by Weidenkaff et al. who performed the reaction in a thermogravimetric analyzer (TGA) to obtain kinetics information [12]. The authors observed that the oxidation was limited by the formation of a zinc oxide layer that prevented access of the water to the unreacted metal in the crucible. Weiss et al. [13]. found conversions as high as 85% by vaporizing the zinc metal ($\Delta H_v = 115\,kJ/mol$) and quenching the vapor with steam. Some of the reaction products deposited inside the reactor during their experiments.

The difficulties of obtaining complete conversion as a result of protective oxide layers suggests, that the kinetics of the hydrogen formation can be improved by reacting small particles at high dispersion in an aerosol. Powders such as the nanometer-sized material collected from the high temperature zinc oxide decomposition reaction limit the oxide layer thickness that has to be penetrated by water for complete conversion. The high heat and mass transfer rates in an aerosol should further promote fast hydrolysis. Since the resulting ZnO will remain in the form of small particles, it can be easily recycled back to the solar high temperature decomposition first step where fine particles are preferred for high dispersion to close the cycle.

This study shows on a laboratory scale that hydrogen can be generated in an aerosol flow reactor by partially hydrolyzing zinc powders at short residence times. Non-isothermal TGA studies confirm that complete conversion should be possible at sufficient residence times in larger-scale reactors. Kinetic parameters were estimated from the TGA results using single-kinetic rate laws and a model-free isoconversional technique and compared with the results of the aerosol reaction.

2. Experimental section

2.1. *Aerosol flow reactor*

The zinc powder aerosol was formed in a commercial fluidized bed feeder (3400A, TSI Inc., Shoreview, MN) using nitrogen as an inert carrier at 6 slpm (4.46 mmol/s). In the feeder, the zinc powder was moved from a reservoir with a bead chain transport mechanism into a fluidized bed of 100 μm sized bronze beads to break zinc agglomerates into primary particles. The small zinc particles were completely elutriated into the gas stream without fractionation while the larger bronze beads remained in the fluidized bed. Steady state flow rates between 1 and 6 g/h with an accuracy of $<10\%$ were achieved after 20–40 min of equilibration time. The feed rate of the fluidized bed feeder at different settings for the bead chain motor was determined prior to the hydrolysis experiments by mounting a filter assembly on a computerized scale and connecting it directly with a short line segment to the feeder. The gas flow rates were controlled with electronic mass flow controllers (Aera, Advanced Energy, Fort Collins, CO). Water was supplied with a syringe pump (NE-1000, New Era Pump Systems, Wantagh, NY), at flow rates from 0 to 30 μl/min through a 0.076 mm I.D. line and mixed with a second nitrogen stream of 1 slpm (0.74 mmol/s) in a temperature-controlled heated zone maintained above 433 K to assure complete vaporization.

Both the preheated zinc and water vapor feed streams were combined at the inlet of a 0.91 m long × 0.019 m I.D. reactor tube that was heated with electrical heat tape. Temperature sensors were installed inside the reactor inlet, at three locations along the external reactor wall and at the feed lines close to the mixing zone to assure even wall temperatures throughout the reaction zone. The zinc feed temperature was limited to <683 K to minimize melting, particle sintering and deposition of liquid zinc on the feed tube walls. The aerosol zinc hydrolysis reaction was performed at a total gas flow rate of 7 slpm (5.21 mmol/s) and reactor wall temperatures between 653 and 813 K at a pressure of 82 kPa. At reactor temperatures above the zinc melting point, both axial and radial temperature gradients in the gas phase were present as the aerosol was heated. Gas residence times in the heated reactor zone between 0.6 and 0.75 s were calculated assuming uniform temperature. These calculations overestimate the residence time for reactor temperatures above the zinc melting point by 1–5% since the average gas temperature is lower due to the temperature profile in the transition region.

A schematic of the experimental setup is shown in Fig. 1. The zinc powder that passed through the reactor was collected in a 0.22 μm HEPA filter (TefSep, GE-Osmonics, Watertown, MA) at the reactor outlet, and the water and hydrogen content of the effluent stream were analyzed with a mass spectrometer (QMS200, SRS, Sunnyvale, CA). The mass spectrometer was calibrated with a 1% hydrogen standard in nitrogen that was diluted with pure nitrogen at different ratios to obtain concentrations similar to those observed in the experiments. The water in the effluent stream caused an elevated but stable hydrogen background in the mass spectrometer that accounted for $<5\%$ of the hydrogen signal from the reaction and was removed by subtraction.

2.2. *TGA*

The TGA was manufactured by Theta Instruments, Inc., Port Washington, NY and was equipped with a high temperature furnace. Consistent results were obtained by dispersing $\sim 15-55$ mg of the zinc powder sample on loosely packed quartz wool that was placed inside a custom crucible with side walls formed from platinum gauze (52 mesh) with a diameter 1.5 cm and a height of 1.6 cm. The surface area of the platinum mesh was calculated to be about 9 cm^2 and 10–15 mg of quartz wool with a BET surface area of 0.88 m^2/g was used. This configuration provided easier access of the water vapor to the sample and also minimized the potential for formation of hot spots as a result of the exothermic reaction. The sample thermocouple was mounted in the center of the furnace tube within 0.5 cm of the sample and heating rates were between ~ 5 and 13 K/min. Moisture was added to the purge stream in a heated vaporization zone using a syringe pump at rates between 4×10^{-5} and 3×10^{-4} mol/min. Overall flow rates through the sample cell were 200 sccm (0.15 mmol/s) at a pressure of 82 kPa. The effluent was analyzed with the same mass spectrometer that was used for the flow reactor experiments to assure stable

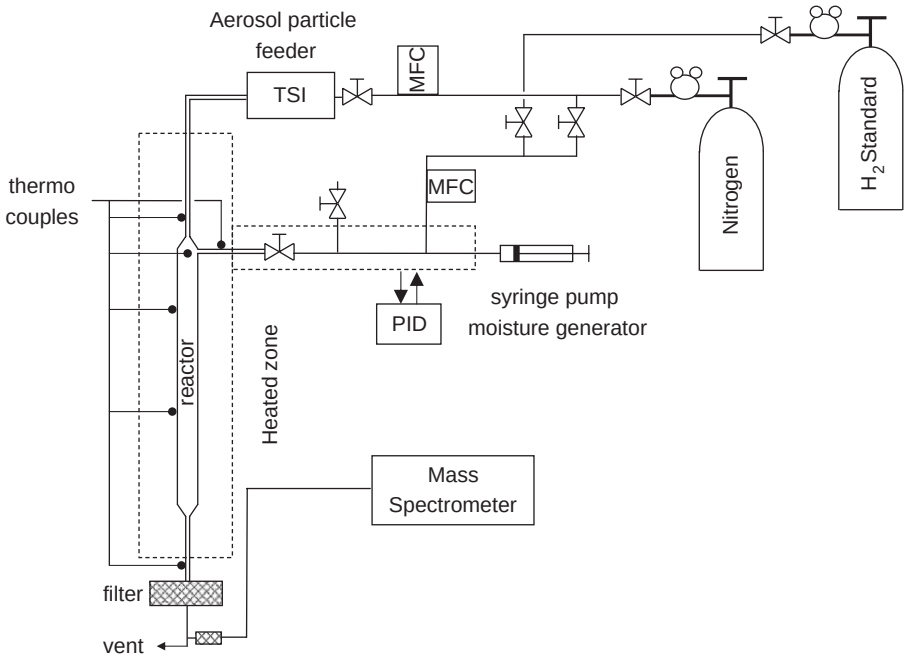

Fig. 1 – Schematic of the aerosol flow reactor setup.

moisture concentrations and a leak-free system as well as to track the hydrogen evolved during the reaction.

2.3. *Product analysis*

The oxygen content of the reaction products was determined with a combustion oxygen analyzer (TC600, LECO Corp., St. Joseph, MI). The instrument was calibrated with a range of standards at similar oxygen concentrations to those found in the products. The particle morphology and oxygen distribution were observed with high resolution transmission electron microscopy (TEM, JSM-7401F, JEOL, Tokyo, Japan)), scanning electron microscopy (SEM, LVSEM, JEOL, Tokyo, Japan) and energy dispersive X-ray spectroscopy (EDS).

2.4. *Chemicals*

The zinc powder had an average particle size of 158 nm (Aldrich #57800-2). The trace metal content was determined by ICP-OES (Table 1). Major impurities were $>2000\,\mu mol/mol$ of copper and $>100\,\mu mol/mol$ of Ni, Mg and Ti.

The air sensitivity of the zinc powder was determined by exposing a sample to the laboratory atmosphere for extended time periods and measuring weight changes on a microbalance and oxidation with the combustion oxygen analyzer. Within the accuracy of the instruments, no such changes were detected even after one month. The inert nature of the powders upon exposure to low humidity air at ambient temperature is consistent with reported corrosion rates as low as $0.2\,\mu m/yr$ for zinc surfaces [14–16]. A thin protective oxide layer was likely present from the manufacturer or from initial air exposure. As an added precaution, the shipping container was handled only in a nitrogen-purged glove bag and air was excluded for all sample transfers.

Table 1 – Trace metal content of zinc powder samples

Trace element	Concentration (μmol/mol)	Instrument detection limit
Cu	2221.46	0.0352
Mg	225.58	0.0041
Ni	171.64	0.0339
Ti	122.60	0.0146
Ca	39.23	0.0132
B	4.90	0.0321
Mn	4.90	0.0104
Cd	DL	0.0000
Ag	DL	0.0018
Al	DL	0.0059
Na	DL	0.0293

The oxygen content of the unreacted material was about 1%. The analysis did not provide information whether the oxygen was evenly distributed throughout the core or was localized on the particle surface. HR-TEM micrographs did not show a defined oxide layer (Fig. 2a) but an estimated layer thickness of ~0.2 nm for a 1% surface oxide shell was too small to be distinguished by the instrument. The surface area was measured with a gas adsorption analyzer (Autosorb AS1, Quantachrome Inc., Boynton Beach, FL) and corresponded to an average particle size that was consistent with the manufacturer specs. SEM images indicated that particle sizes ranged from ~50–250 (Fig. 2b).

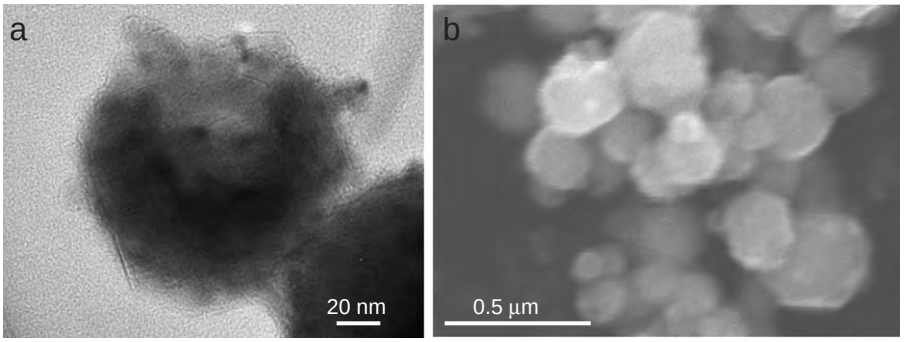

Fig. 2 – Images of nano-sized zinc powder: (a) TEM and (b) SEM.

3. Results and discussion

3.1. TGA studies

The hydrolysis of the zinc powder in a TGA provided insight into the intrinsic reaction kinetics under controlled operating conditions. All measurements were performed in the non-isothermal mode where water was added to the purge stream and a heating ramp was initiated after water concentrations were stabilized. Since the reaction is first observed below 550 K, a significant fraction of the particles was oxidized as the melting point of 713 K was approached and coalescence was not observed at higher temperatures. A typical result obtained with a dispersed sample of 54.9 mg zinc powder at a heating rate of 11.9 K/min and a water concentration of 1.5 vol% is shown in Fig. 3. The derivative signal shows a single peak, consistent with an activated reaction where the conversion rate first increases with temperature and then drops as the reactant is depleted. The sample mass did not have any significant effect on the overall kinetics as shown in Fig. 4 where two samples of 14.8 and 54.9 mg are compared with an $R^2 = 0.9948$. The signal noise was larger for the smaller sample as the detection limit of the instrument was approached but dispersion of more than about 30 mg on the quartz wool support was difficult due to a lack of adhesion of the zinc particles and average sample sizes were between 20 and 30 mg. The benefits of small samples include improved heat dissipation and minimized diffusion boundaries.

Water concentrations below about 0.4 vol% caused distortions of the sigmoidal conversion curves as a result of limited water availability but above about 0.7 vol% no effect of the water concentration was found. Measurements were therefore carried out at 1.5 vol%. Higher concentrations were not possible due to cooling jackets of the high temperature furnace that would have caused condensation at the furnace inlet. The water feed of 1.6×10^{-4} mol/min at sample sizes of $\sim 3-4 \times 10^{-4}$ mol zinc assured sufficient water availability.

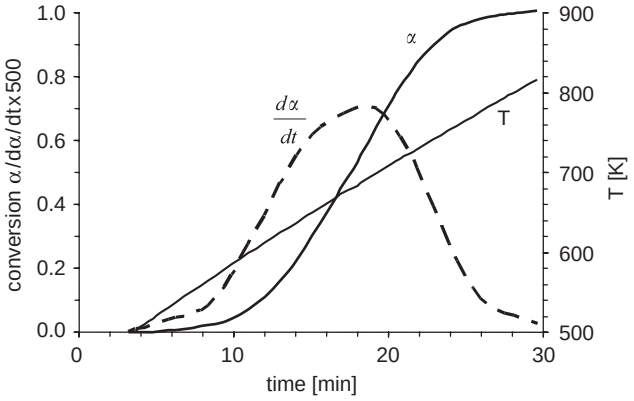

Fig. 3 – Hydrolysis of 54.9 mg nano-sized zinc powder at a heating rate of 11.9 K/min and a water concentration of 1.5 vol% in the TGA—sample dispersed on quartz wool in wire mesh crucible.

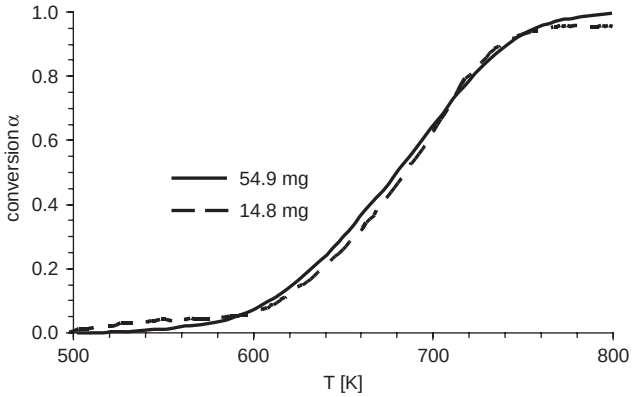

Fig. 4 – TGA measurements with 14.8 and 54.9 mg samples at a heating rate of 11.9 K/min.

3.2. Kinetic analysis

TGA data were analyzed using two different approaches.

3.2.1. Single-step kinetics

The experimental data were fitted to a single-step kinetic equation that decouples the Arrhenius-type activated process and a model-dependent depletion term $f(\alpha)$ where α is the fractional conversion [17]:

$$\frac{d\alpha}{dt} = \beta\frac{d\alpha}{dT} = A_0 e^{-E_A/RT} f(\alpha). \quad (3)$$

β is the heating rate:

$$\beta = \frac{dT}{dt}. \quad (4)$$

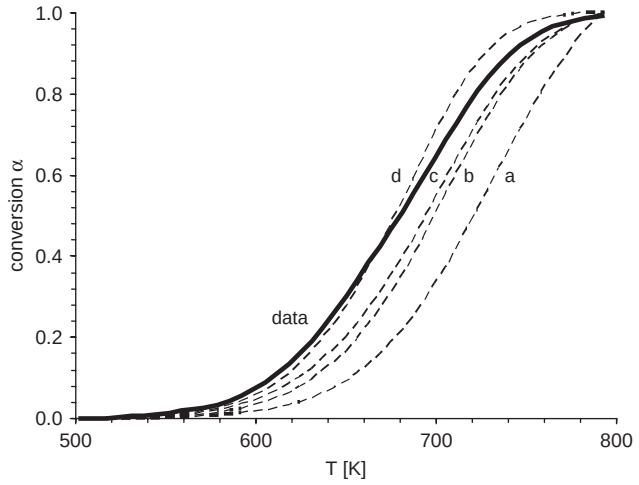

Fig. 5 – Comparison of experimental data from Fig. 3 with predictions using different reaction models $f(\alpha)$: (a) $3(1-\alpha)^{2/3}$; (b) $3(1-\alpha)^{2/3}+2(1-\alpha)$; (c): $(1-\alpha)^n$, $n=0.4$ and (d) $(1-\alpha)^n$, $n=1.6$.

Fig. 5 shows the comparison of the measurements in Fig. 3 with Eq. (3) using different functions $f(\alpha)$ for the reaction model. The model parameters were determined by regression. The TGA signal was best described by an order of reaction term with an activation energy of 112 kJ/mol for an empirical fit: $f(\alpha)=(1-\alpha)^n (n\sim 1.6,\ R^2=0.996)$. Also shown are three other reaction models using the same activation energy for better comparison. Adjusting the activation energy did not improve the model predictions, likely because of compensation effects where A_0 and E_a appear to be correlated [18]. The more likely shrinking core model [19] where a growing porous or non-porous ash layer of zinc oxide forms around an unreacted metal core and diffusion limitations of water or zinc ions are considered ($f(\alpha)=3(1-\alpha)^{2/3}+2(1-\alpha)$) did not fit the data as well ($R^2=0.901$). An exponential model ($f(\alpha)=1-\alpha^n$ ($n\sim 0.4$, $R^2=0.928$), and a contracting sphere model $f(\alpha)=3(1-\alpha)^{2/3}$ ($R^2=0.755$) also did not match the experimental results.

The single-step kinetic models were derived under the assumption of uniform particle sizes and are therefore not expected to be accurate for the wide size distribution in the samples used for this study. Also, changes in reaction mechanisms from faster surface reactions in the early stage of conversion to a diffusion-limited process is likely but is not accounted for by this method. In addition, the hydrolysis reaction is strongly exothermic and localized hot spots cannot be ruled out even though care was taken to optimize heat dissipation by dispersing the sample on quartz wool and locating the temperature sensor close to the sample.

Since the calculated activation energies can be a strong function of $f(\alpha)$[20] and the best fits were obtained with an empirical reaction model that did not provide any insight into the reaction mechanism, the physical significance of the activation energies calculated by the single-kinetics model was doubtful. Therefore, a model-free approach was applied to determine activation energies that are independent of the model assumptions.

3.2.2. *Model-free isoconversional method at different heating rates*

The isoconversional method has been shown to provide activation energies without the need for a reaction model [20]. An integrated form of Eq. (3) is used that is independent of $f(\alpha)$:

$$g(\alpha)\equiv\int_0^{\alpha}\frac{d\alpha}{f(\alpha)}=\frac{A}{\beta}\int_0^{T_\alpha}e^{-E/RT}\,dT=\frac{AI(E,T)}{\beta}, \tag{5}$$

$I(E,T)$ is the temperature integral. Since the integral over $1/f(\alpha)$ and therefore $g(\alpha)$ does not change with β, a set of experiments at different heating rates can be used to calculate activation energies as a function of conversion. At a given conversion, it follows with different heating rates $\beta_I(i=1,\ldots n)$ that

$$g(\alpha)=\frac{A_\alpha I(E_\alpha,T_{\alpha,1})}{\beta_1}=\frac{A_\alpha I(E_\alpha,T_{\alpha,2})}{\beta_2}=\cdots=\frac{A_\alpha I(E_\alpha,T_{\alpha,n})}{\beta_n}. \tag{6}$$

The activation energy at α does not depend on $f(\alpha)$ and can then be determined by minimizing the following variance:

$$S^2(E_\alpha)=\frac{1}{n(n-1)}\sum_{i=1}^{n}\sum_{j\neq i}^{n}\left[\frac{A_\alpha I(E_\alpha,T_{\alpha,i})/\beta_i}{A_\alpha I(E_\alpha,T_{\alpha,j})/\beta_j}-1\right]^2. \tag{7}$$

The confidence limits for E_α can be calculated from the confidence limits of the variance at the optimum value of the activation energy using the F-distribution [20]. The temperature integrals were obtained by numerical integration. Fig. 6 shows measurements at heating rates of 5.3, 9 and 12.3 K/min. Activation energies showed a minimum of about 106 kJ/mol at 60–70% conversion and increased at higher and lower conversions with an average of 132 ± 27 kJ/mol between 30 and 70% conversion (Fig. 7). The 90% confidence intervals show high levels of uncertainty at high and low conversions due to the instrument fluctuations that are more influential during the initial and final stages of the measurements where mass changes are small.

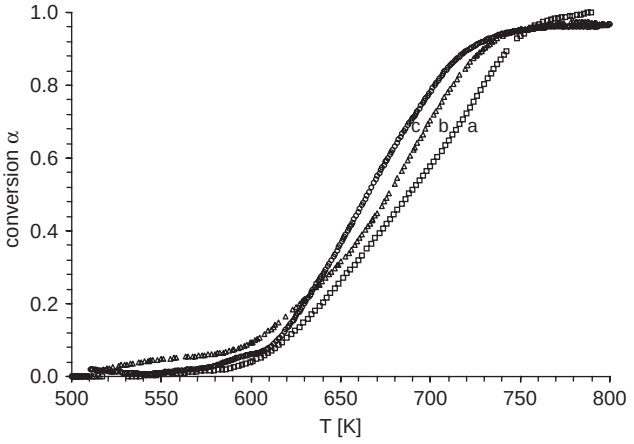

Fig. 6 – Hydrolysis of three samples of about 20 mg dispersed on quartz wool in a wire mesh cage at different heating rates and a water concentration of 1.5 vol%: (a) 5.3 K/min (23.3 mg); (b) 9 K/min (25.9 mg) and (c) 12.3 K/min (19.5 mg).

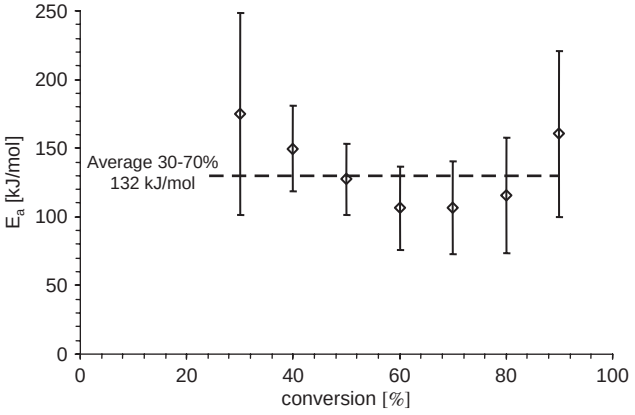

Fig. 7 – Activation energy as function of conversion determined by isoconversion method from data in Fig. 6.

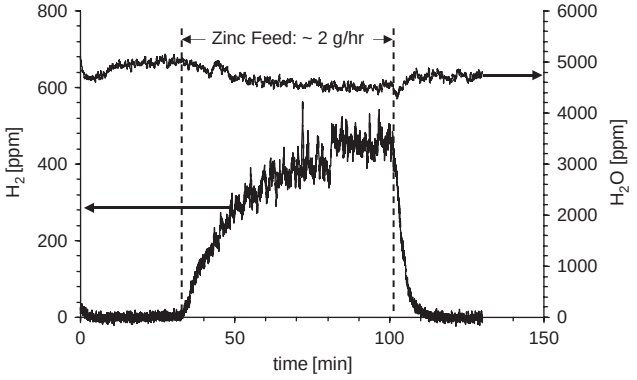

Fig. 8 – H_2 and H_2O concentration in flow reactor effluent during hydrolysis of nano-sized zinc powder at ~703 K, a particle feed rate of ~2 g/h and a gas flow rate of 7 l(STP)/min (5.21 mmol/s).

The pre-exponential factor can then be determined by regression, again requiring the use of a reaction model. With the previously determined empirical best fit $f(\alpha) = (1-\alpha)^n$, $A_0 = 5.6 \times 10^9 \pm 0.3 \times 10^9\,\mathrm{min}^{-1}$ for the measurements shown in Fig. 6 with $n = 1.73$.

Activation energies in the range of 110–130 kJ/mol for zinc hydrolysis are higher than previously reported for zinc foils [15] and molten zinc [11] but consistent with the oxidation of zinc by oxygen [21,22]. Both the diffusion of O^{2-} and Zn^{2+} ions have been discussed as the limiting factor and oxidation by water might be similar if the surface adsorption and dissociation is fast compared to the bulk diffusion of either zinc or oxygen ions. In addition, trace contaminants have been shown to strongly affect oxidation and diffusion behavior [23]. High activation energies compared to previous studies with water might therefore be due to differences in the powder composition [12] since the zinc used in this study contained about >2000 μmol/mol copper and >100 μmol/mol of Mg, Ni and Ti.

The results of the TGA measurements confirm that complete conversion of nano-sized zinc particles to zinc oxide by water vapor is possible within a few minutes at temperatures above 650 K. Even though conclusions that could be drawn about the mechanism of this reaction were limited, average model-independent activation energies of ~132 kJ/mol were derived from the measurements at different heating rates.

3.3. *Flow tube reactor*

The flow measurements confirm that fast reaction is possible with a zinc powder aerosol. Even though the temperature of the aerosol pre-heater line was limited to the melting point of zinc to prevent deposition, coalescence and increased particle sizes, final reaction temperatures in the reactor that exceeded this limit were possible since a protective oxide layer was rapidly formed at the inlet upon mixing with water vapor.

The mass spectrometer response for a typical experiment at ~723 K is shown in Fig. 8. As the zinc powder is added to the gas stream at a rate of 5.1×10^{-4} mol/min by turning the feeding mechanism of the fluidized bed feeder on, a corresponding increase in the hydrogen signal is observed. An equilibration time of ~30–40 min that is similar to the time for the particle feeder to stabilize was observed before the hydrogen reached steady state. The hydrogen concentration of ~450 ppm at 7 slpm (5.21 mmol/s) N_2 flow corresponds to $\sim 1.4 \times 10^{-4}$ mol/min hydrogen formation or ~27% conversion based on the zinc feed. This conversion overestimates the true reaction rate of the particles that remain suspended in the gas phase since accumulating particles on the reactor wall will continue to hydrolyze with the excess water under hydrogen release until complete conversion and add to the overall hydrogen signal. The water concentration trace shows a drop that is consistent with the observed hydrogen levels within the scatter of the reading as predicted by the stoichiometry of the reaction.

The HEPA particle filter at the reactor outlet was placed on a scale to track the mass of the collected particles on-line, which provided a qualitative measure of the progress of the experiment. Since it has been shown that even unreacted particles were protected by their native oxide layer, no further reaction was assumed in the filter that was at ambient temperature. However, quantitative material balances were not possible as a result of particle deposition inside the feed lines and reactor walls during the experiment. Comparing the mass gain of the filter when connected directly to the outlet of the particle feeder with the measurements where the reactor was in-line indicated that the particle deposition was 10–30% of the overall feed rate. Even though powder accumulation is a challenge for small laboratory reactors, loosely adhering particle layers could be removed mechanically in a scaled-up system and the thickness of such buildup will be limited by weak adhesion forces.

The reacted particles in the filter were darker in color than the light-gray precursor, likely a sign of partial oxidation. Average particle size was similar to that of unreacted powder. Cross-sectional TEM images of the product particles combined with EDS revealed the formation of a zinc oxide layer surrounding a zinc metal core (Fig. 9). The material in the filter was assumed to be representative of the material that flowed through the reaction zone for the duration of the

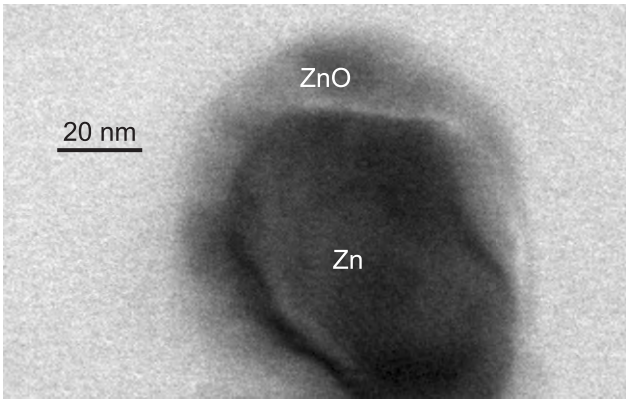

Fig. 9 – TEM image of nano-zinc reacted at 733 K.

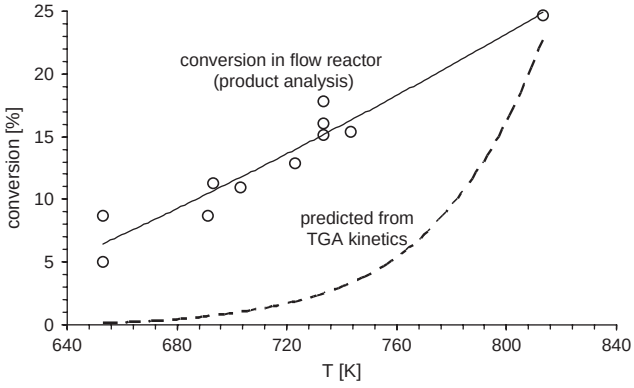

Fig. 10 – Measured and predicted conversions of nano-sized zinc powder in the aerosol flow reactor.

calculated gas residence time. Combustion oxygen analysis was then used to calculate overall conversions. The samples collected in the filter for the experiment in Fig. 8 showed only 11% conversion compared to a calculated conversion of 27% based on evolved hydrogen that included the hydrogen evolution from particles accumulated on the reactor walls. Samples collected from the reactor walls after the experiments were completely oxidized as expected after several hours of water vapor exposure at reaction temperature.

Overall conversions in the flow reactor determined from the product oxygen content increase with increasing temperature (Fig. 10). The dashed line in Fig. 10 shows conversions calculated from the TGA parameters by integrating Eq. (3) at similar residence times and reaction temperatures to the flow experiments. The predicted conversions at lower temperatures are much lower than the measured values, but the discrepancy decreases as the temperature rises. At the highest temperature with a residence time of ~0.6 s, the conversions for the flow experiments were similar to the modeling results. The TGA kinetics predicts that 95% of the zinc could be oxidized in about 2 s at 813 K or <1 min at 683 K. Such extrapolation is obviously of limited accuracy as a result of the discussed uncertainty of the models but could provide a rough estimate for the range of residence times that are likely required for high conversions.

Improved mass and heat transfer for the finely dispersed and diluted aerosol particles as compared to the suspended particles in the TGA are likely explanations for the higher conversions in the flow experiments at lower temperatures. Also, since a significant fraction of the particles in the flow reactor is oxidized in less than 1 s, the heat of reaction released during this rapid conversion could result in increased particle temperatures. Localized heating of the particles could not be detected with the experimental setup. Based on the feed flow rates and measured conversion in the reactor, an average temperature increase $<5\,^{\circ}C$ due to the heat of reaction was calculated for a wall temperature of 813 K. Rapid heating might also cause cracking of the zinc oxide layer that forms during the reaction and improve access to the unreacted zinc core. In the TGA experiments, heating rates are much slower and increased heating of the particles as a result of rapid conversion is less likely. Even though a more quantitative understanding of the inter- and intra-particle transport resistances, intrinsic kinetic rate laws, and the influence of the reactor design is desirable, this first-pass study supports the assumption that the kinetics of the zinc hydrolysis can be enhanced in an aerosol reactor.

4. Conclusions

The combination of aerosol flow reactor measurements and the kinetic analysis of TGA data provided the opportunity to compare the performance of a bench scale system for continuous hydrogen formation by zinc powder aerosol hydrolysis with independently measured empirical kinetic rate laws. The aerosol flow system showed higher conversions than predicted from the TGA kinetics which is likely due to increased mass and heat transfer. The TGA results verified that complete conversion is possible for sub-micron-sized particles, but in a flow reactor, longer residence times than those of the bench system and measures to prevent buildup will be required.

Acknowledgments

We gratefully acknowledge the DOE hydrogen initiative (DOE DE-PS36-03GO93007) for their financial support. The authors would like to thank Thomas Giddings for his assistance in preparing the cross-sectional TEM samples.

REFERENCES

[1] Perkins C, Weimer AW. Likely near-term solar-thermal water splitting technologies. Int J Hydrogen Energy 2004;29:1587.
[2] Bilgen E, Bilgen C. Solar hydrogen production using two-step thermochemical cycles. Int J Hydrogen Energy 1982;7:637.
[3] Palumbo R, Lédé J, Boutin O, Elorza Ricart E, Steinfeld A, Möller S, et al. The production of Zn from ZnO in a high-temperature solar decomposition quench process—I. The scientific framework for the process. Chem Eng Sci 1998;53:2503.
[4] Steinfeld A. Solar hydrogen production via a two-step water-splitting thermochemical cycle based on Zn/ZnO redox reactions. Int J Hydrogen Energy 20002;27:611.

[5] Weidenkaff A, Steinfeld A, Wokaun A, Auer PO, Eichler B, Reller A. Direct solar thermal dissociation of zinc oxide: condensation and crystallization of zinc in the presence of oxygen. Sol Energy 1999;65:59.
[6] Steinfeld A, Brack M, Meier A, Weidenkaff A, Wuillemin D. A solar chemical reactor for co-production of zinc and synthesis gas. Energy 1998;23:803.
[7] Steinfeld A, Frei A, Kuhn P, Wuillemin D. Solar thermal production of zinc and syngas via combined ZnO-reduction and CH4-reforming process. Int J Hydrogen Energy 1995;20:793.
[8] Osinga T, Frommherz U, Steinfeld A, Wieckert C. Experimental investigation of the solar carbothermic reduction of ZnO using a two-cavity solar reactor. J Sol Energy Eng 2004;126:633.
[9] Berman A, Epstein M. The kinetic model for carboreduction of zinc oxide. J Phys IV Proc 1999;9:Pr3/319.
[10] Kräupl S, Steinfeld A. Experimental investigation of a vortex-flow solar chemical reactor for the combined ZnO-reduction and CH4-reforming. J Sol Energy Eng 2001;123:237.
[11] Berman A, Epstein M. The kinetics of hydrogen production in the oxidation of liquid zinc with water vapor. Int J Hydrogen Energy 2000;25:957.
[12] Weidenkaff A, Reller AW, Wokaun A, Steinfeld A. Thermogravimetric analysis of the ZnO/Zn water splitting cycle. Thermochim Acta 2000;359:69.
[13] Weiss RJ, Ly HC, Wegner K, Pratsinis SE, Steinfeld A. H_2 production by Zn hydrolysis in hot-wall aerosol reactor. AICHE J 2005;51:1966.
[14] Alimenti GA, Gschaider ME, Bazán JC, Ferreira ML. Theoretical and experimental study of the interaction of O_2 and H_2O with metallic zinc—discussion of the initial step of oxide formation. J Colloid Interface Sci 2004;276:24.
[15] Bazán JC, Gschaider ME, Alimenti GA. Gravimetric study of interaction of water vapor with metallic zinc. J Therm Anal Calorimetry 1999;55:569.
[16] Graedel TE. Corrosion mechanisms for zinc exposed to the atmosphere. J Electrochem Soc 1989;136:193C.
[17] Brown ME, Maciejewski M, Vyazovkin S, Nomen R, Sempere J, Burnham A, et al. Computational aspects of kinetic analysis part A: the ICTAC kinetics project-data, methods and results. Thermochim Acta 2000;355:125.
[18] Eisenreich N. Direct least squares fit of chemical reaction curves and its relation to the kinetic compensation effect. J Therm Anal 1980;19:289.
[19] Levenspiel O. Chemical reaction engineering. 3rd ed. New York: Wiley; 1998.
[20] Vyazovkin S, Wight CA. Estimating realistic confidence intervals for the activation energy determined from thermoanalytical measurements. Anal Chem 2000;72:3171.
[21] Moore WJ, Lee JK. Kinetics of the formation of oxide films on zinc foil. Trans Faraday Soc 1951;47:501.
[22] Delalu H, Vignalou JR, Elkhatib M, Metz R. Kinetics and modeling of diffusion phenomena occurring during the complete oxidation of zinc powder: influence of granulometry temperature and relative humidity of the oxidizing fluid. Solid State Sci 2000;2:229.
[23] Tomlins GW, Routbort JL, Mason TO. Zinc self-diffusion, electrical properties, and defect structure of undoped, single crystal zinc oxide. J Appl Phys 2000;87:117.